LISA observations of rapidly spinning massive black hole binary systems

Alberto Vecchio

School of Physics and Astronomy, The University of Birmingham, Edgbaston, Birmingham B15 2TT, United Kingdom
(Received 28 February 2003; published 17 August 2004)

Binary systems of massive black holes will be detectable by the Laser Interferometer Space Antenna (LISA) throughout the entire Universe. Observations of gravitational waves from this class of sources will have important repercussions on our understanding of the behavior of gravity in the highly nonlinear relativistic regime, the distribution and interaction of massive black holes at high redshift, and the formation and evolution of cosmic structures. It is therefore important to address how accurately LISA can measure the source parameters and explore the implications for astronomy and cosmology. Present observations and theoretical models suggest that massive black holes could be spinning, possibly rapidly in some cases. In binary systems, the relativistic spin-orbit interaction causes the orbital plane to precess in space, producing a characteristic signature on the emitted gravitational waves. In this paper we investigate the effect of spins on the gravitational wave signal registered at the LISA output—we provide ready-to-use analytical expressions of the measured signal—and the implications for parameter estimation. We consider the inspiral phase of binary systems in circular orbit undergoing the so-called ''simple precession'' and we approximate the gravitational radiation at the restricted post$^{1.5}$-Newtonian order. We show that the presence of spins changes dramatically the signature of the signal recorded by LISA. As a consequence, the mean square errors associated with the parameter measurements are significantly smaller than the ones obtained when the effect of spins is neglected. For a binary system of two $10^6 M_\odot$ black holes, the angular resolution and the relative error on the luminosity distance improve by a factor of ≈ 3–10; the fractional errors on the chirp mass and the reduced mass decrease by a factor of ~ 10 and $\sim 10^3$, respectively.

I. INTRODUCTION

Binary systems of massive black holes in the mass range $10^5 M_\odot$–$10^7 M_\odot$ are among the most spectacular sources that will be observed by the Laser Interferometer Space Antenna (LISA), an ESA/NASA space-borne laser interferometer aimed at observations of gravitational waves (GWs) in the low-frequency region of the spectrum, $\sim 10^{-5}$–0.1 Hz, and expected to be launched in 2011 [1]. The interest in the detection of gravitational radiation from massive black holes (MBHs) is twofold [2]: (i) for fundamental physics, because it will provide a thorough understanding of the behavior of strong gravity in the highly nonlinear relativistic regime and (ii) for astronomy and cosmology because GWs provide an ''orthogonal'' and complementary mean, with respect to conventional astronomy, of investigating the high-redshift formation and evolution of cosmic structures, such as galaxy interactions and mergers, and exploring the demography of massive black holes.

Massive black holes are considered to be essentially ubiquitous in the center of galaxies in the local and low-redshift universe [3,4]. Our galaxy [5] and NGC 4258 [6] provide probably the most solid observational evidence for the existence of such black holes [7]. Evidence for the presence of black holes in galaxies at high redshift is more circumstantial, but the fact that galaxies, at some stage of their life, harbor AGNs and that we observe quasars at $z \gtrsim 6$ [8] strongly favors the hypothesis that black holes are fairly common also at high redshift. This conclusion is supported by recent results [9] that show that the high-redshift quasar distribution and the present day density of black holes can be reconciled by invoking galaxy mergers where the relation between host velocity dispersion and black hole mass is consistent with the one observed locally [10]. The present day population of MBHs is therefore likely to be the dormant remnant of those earlier activities. Two black holes are brought together at the center of a merger remnant by dynamical friction from the stars of the common host. The further evolution of a binary must then take place on a time scale short enough for the system to coalesce within a Hubble time due to radiation reaction. Two are the main mechanisms that could make the binary hard enough to satisfy this condition: dynamical friction from stars in the core [11–15] and gas dynamical effects [16,17]. However, despite all this circumstantial evidence, the rate of coalescence of massive black hole binaries in the Universe is still controversial: present astrophysical estimations vary widely from ~ 0.1 to ~ 100 yr^{-1} [11,18–24], depending on model assumptions and BH mass range. At present there is no direct observational evidence for the presence of massive black hole binary systems, with the possible exception of OJ287 [25].

LISA will be able to detect MBH binaries at a moderate-to-high signal-to-noise ratio throughout the entire Universe (redshift $z \approx 10$ and beyond, if black holes are already present). During the whole LISA observational campaign—the nominal duration of the mission is 3 years, but the instrument is expected to operate for about 10 years, if no catastrophic failure occurs on the spacecraft—one can therefore expect from a few to a very large number of detections.

LISA is an all-sky monitor. At any one time, the instrument maps the whole sky, although with a different sensitivity depending on the location of the source and the polarization of the waves. By coherently tracking the phase and

amplitude evolution of GWs, one can extract precise information about a source. In observations of binary systems, the number of parameters on which the waveform depends, and that one needs to extract from the data, is large, in the most general case 17. Clearly correlations among parameters are inevitable, degrading the precision of the measurements.

A few studies have been carried out so far to address how accurately LISA can measure the source parameters and the implications for astronomy and cosmology. Because of the complexity of the problem and open theoretical issues in the modeling of the gravitational waveform in the most general case, assumptions, possibly *ad hoc*, have been introduced on the waveform model. Cutler [26] has considered the inspiral phase of binary systems approximating the waveform at the restricted post$^{1.5}$-Newtonian order. Sintes and Vecchio [27,28] and Moore and Hellings [29] have investigated the parameter estimation including post^2-Newtonian corrections to the amplitude and the phase. Hughes [30] has considered restricted post^2-Newtonian waveforms for the inspiral phase and has included the ringdown portion of the signal; more recently, Seto has included the effect of the finite length of the LISA arms using restricted post$^{1.5}$-Newtonian waveforms [31]. All these analyses have *a priori* assumed that black holes have no spins or the spins are parallel to each other and the orbital angular momentum. However, present astrophysical observations and theoretical models suggest that massive black holes are likely to be rotating, possibly rapidly in some cases. Observations of AGNs and quasars are highly consistent with rapidly rotating black holes; observations of black holes in quiescence are in agreement with a slow, if any, rotation and some theoretical models suggest small-to-moderate spins (see, e.g., [32]). If there is little doubt that black holes are, in general, rotating, how strong spins are is to a large extent unknown. Quite likely, gravitational wave observations shall provide the most effective tool in addressing this issue. Spins are likely to add vast complexity to the signal recorded at the detector output and require more parameters to describe the waveform [33–36]. In this paper we show that spins do change dramatically the structure of the signal observed by LISA and, as a consequence, affect significantly (even by orders of magnitudes for some selected parameters) the errors with which LISA can measure the source parameters.

In this paper we restrict our attention to the inspiral phase of massive binary systems of comparable mass. We consider circular orbits, model the waveform at the restricted post$^{1.5}$-Newtonian order, and assume that binary systems undergo the so-called *simple precession* [33], which is the relevant scenario from an astrophysical viewpoint. The goal of the paper is twofold: (i) to provide ready-to-use analytical expressions for the LISA detector output when binary systems undergo spin-orbit precession and (ii) to show the dramatic change in parameter estimation that occurs when spin-orbit modulation in phase and amplitude is taken into account. The actual parameter space is so vast—the waveform is described by 12 parameters—that here we concentrate on typical systems of two $10^6 M_\odot$ black holes. A thorough exploration of the whole parameter space requires large-scale, CPU-intensive Monte Carlo simulations and is

beyond the scope of this paper; such analysis is currently in progress and will be reported in a separate paper [37].

The organization of the paper is as follows. In Sec. II we review the main features of the LISA mission, in particular its orbital configuration which is central for the topic discussed in this paper. In Sec. III we review the main properties and key equations regarding the emission of GWs from inspiraling binary systems, with emphasis on the role played by spins, and we stress the differences with respect to the nonspinning—i.e., nonprecessing—case. Sections IV and V contain the key results of the paper. In Sec. IV we derive explicit ready-to-use analytical expressions for the signal measured at the LISA detector output for binary systems in circular orbit that undergo simple precession; the waveform is computed within the restricted post$^{1.5}$-Newtonian approximation. In Sec. V we explore the errors with which the 12 parameters of the signal can be determined and compare the results with the case where spins are neglected. In Sec. VI we summarize our conclusions and present pointers to future work.

II. LISA MISSION

In this section we review the main properties of the LISA mission. We refer the reader to [1] for more details.

A. LISA orbit

LISA is an all-sky monitor with a quadrupolar antenna pattern. Its orbital configuration is conceived in order to keep the geometry of the interferometer as stable as possible during the mission, which in turn provides a thorough coverage of the whole sky: a constellation of three drag-free spacecraft (containing the "free-falling test masses") is placed at the vertexes of an ideal equilateral triangle with sides $\simeq 5 \times 10^6$ km; it forms a three-arm interferometer, with a 60° angle between two adjacent laser beams. The LISA orbital motion is as follows: the barycenter of the instrument follows an essentially circular heliocentric orbit, 20° behind the Earth; the detector plane is tilted by 60° with respect to the Ecliptic and the instrument counterrotates around the normal to the detector plane with the same period 1 yr.

Following [26] we introduce two Cartesian reference frames [38]: (i) a fixed "barycentric" frame (x, y, z) tied to the Ecliptic and centered in the solar system barycenter, with $\hat{\mathbf{z}}$ perpendicular to the ecliptic, and the plane (x, y) in the ecliptic itself; (ii) a detector reference frame (x', y', z'), centered in the LISA center of mass and attached to the detector, with $\hat{\mathbf{z}}'$ perpendicular to the plane defined by the three arms and the x' and y' axes defined so that the unit vectors $\hat{\mathbf{l}}_j$ ($j = 1, 2, 3$) along each arm read

$$\hat{\mathbf{l}}_j = \cos\left[\frac{\pi}{12} + \frac{\pi}{3}(j-1)\right]\hat{\mathbf{x}}' + \sin\left[\frac{\pi}{12} + \frac{\pi}{3}(j-1)\right]\hat{\mathbf{y}}'. \quad (1)$$

In the ecliptic frame the motion of LISA's center of mass is described by the polar angles

$$\Theta = \frac{\pi}{2},$$

$$\Phi(t) = \Phi_0 + n_\oplus t, \tag{2}$$

where

$$n_\oplus \equiv \frac{2\pi}{1 \text{ yr}}, \tag{3}$$

and Φ_0 sets the position of the detector at same arbitrary reference time. The normal to the detector plane $\hat{\mathbf{z}}'$ precesses around $\hat{\mathbf{z}}$ according to

$$\hat{\mathbf{z}}' = \frac{1}{2}\hat{\mathbf{z}} - \frac{\sqrt{3}}{2}[\cos\Phi(t)\hat{\mathbf{x}} + \sin\Phi(t)\hat{\mathbf{y}}]. \tag{4}$$

The time evolution of the unit vectors $\hat{\mathbf{l}}_j$ ($j=1,2,3$) along each arm is described by the expression [26]

$$\hat{\mathbf{l}}_j = \left[\frac{1}{2}\sin\alpha_j(t)\cos\Phi(t) - \cos\alpha_j(t)\sin\Phi(t)\right]\hat{\mathbf{x}}$$
$$+ \left[\frac{1}{2}\sin\alpha_j(t)\sin\Phi(t) + \cos\alpha_j(t)\cos\Phi(t)\right]\hat{\mathbf{y}}$$
$$+ \left[\frac{\sqrt{3}}{2}\sin\alpha_j(t)\right]\hat{\mathbf{z}}, \tag{5}$$

where $\alpha_j(t)$ increases linearly with time, according to

$$\alpha_j(t) = n_\oplus t - (j-1)\pi/3 + \alpha_0, \tag{6}$$

and α_0 is just a constant specifying the orientation of the arms at the arbitrary reference time $t=0$.

B. LISA detector output

The strain $h(t)$ produced at the output of the LISA Michelson interferometer by a GW signal characterized by the two independent polarization states $h_+(t)$ and $h_\times(t)$ [42] is

$$h^{(\iota)}(t) = \frac{\sqrt{3}}{2}[F_+^{(\iota)}(t)h_+(t) + F_\times^{(\iota)}(t)h_\times(t)]. \tag{7}$$

In Eq. (7), $F_+^{(\iota)}(t)$ and $F_\times^{(\iota)}(t)$ are the *time-dependent* antenna patters and the factor $\sqrt{3}/2 = \sin(\pi/3)$ comes from the 60° opening angle of the LISA arms. F_+ and $F_\times$ vary with time because during the observation the interferometer changes orientation with respect to the source; in fact, inspiral binaries are long-lived sources in the low-frequency band. The index $\iota=$I,II labels the two independent Michelson outputs that can be constructed from the readouts of the three arms if the noise is uncorrelated and "totally symmetric" [26]. They are equivalent to the outputs of two identical interferometers in the same location, rotated by 45° one with respect to the other.

The functions describing the interferometer beam pattern depend on the source location in the sky $\hat{\mathbf{N}}$ (GWs propagate in the $-\hat{\mathbf{N}}$ direction) and wave polarization, which is related to the orientation of the orbital plane, and therefore the orbital angular momentum $\hat{\mathbf{L}}$, with respect to the detector. With respect to the frame tied to the solar system barycenter, $\hat{\mathbf{N}}$ and $\hat{\mathbf{L}}$ are described by the polar angles (θ_N, ϕ_N) and (θ_L, ϕ_L). Equivalently, in the frame attached to the detector, $\hat{\mathbf{N}}$ and $\hat{\mathbf{L}}$ are identified by the angles (θ_N', ϕ_N') and (θ_L', ϕ_L'). In the reference frame attached to LISA, the antenna beam patterns read

$$F_+(\theta_N', \phi_N'\psi_N') = \frac{1}{2}(1 + \cos\theta_N'^2)\cos 2\phi_N'\cos 2\psi_N'$$
$$- \cos\theta_N'\sin 2\phi_N'\sin 2\psi_N', \tag{8a}$$

$$F_\times(\theta_N', \phi_N'\psi_N') = \frac{1}{2}(1 + \cos\theta_N'^2)\cos 2\phi_N'\sin 2\psi_N'$$
$$+ \cos\theta_N'\sin 2\phi_N'\cos 2\psi_N', \tag{8b}$$

where ψ_N' describes the "polarization angle" of the waveform in the detector frame. The antenna patterns (8a) and (8b) for the two outputs $\iota=$I and $\iota=$II are, therefore,

$$F_{+,\times}^{(\iota)}(t) = \begin{cases} F_{+,\times}(\theta_N', \phi_N'\psi_N') & (\iota = \text{I}), \\ F_{+,\times}(\theta_N', (\phi_N' - \pi/4), \psi_N') & (\iota = \text{II}). \end{cases} \tag{9}$$

Note that because of the detector change of orientation, the angles θ_N', ϕ_N', and ψ_N' are time dependent. As a function of the angles measured in the solar system barycenter they read

$$\cos\theta_N'(t) = \frac{1}{2}\cos\theta_N - \frac{\sqrt{3}}{2}\sin\theta_N\cos[\Phi(t) - \phi_N], \tag{10}$$

$$\phi_N'(t) = \Xi_1 + \frac{\pi}{12}$$
$$+ \tan^{-1}\left\{\frac{\frac{\sqrt{3}}{2}\cos\theta_N + \frac{1}{2}\sin\theta_N\sin[\Phi(t) - \phi_N]}{\sin\theta_N\sin[\Phi(t) - \phi_N]}\right\}, \tag{11}$$

$$\tan\psi_N' = \frac{\hat{\mathbf{L}}\cdot\hat{\mathbf{z}}' - (\hat{\mathbf{L}}\cdot\hat{\mathbf{N}})(\hat{\mathbf{z}}'\cdot\hat{\mathbf{N}})}{\hat{\mathbf{N}}\cdot(\hat{\mathbf{L}}\times\hat{\mathbf{z}}')}, \tag{12}$$

where

$$\Xi_j = n_\oplus t - \frac{\pi}{12} - \frac{\pi}{3}(j-1) + \Xi_0, \tag{13}$$

and Ξ_0 sets the orientation of $\hat{\mathbf{l}}_j$ at $t=0$. We are not yet ready to derive the explicit expression for ψ_N', Eq. (12), because for spinning black holes, the source at the center of this paper, $\hat{\mathbf{L}}$ is not a constant of motion. We derive the necessary equations in the following section.

III. GRAVITATIONAL WAVES FROM BINARY SYSTEMS

In this section we briefly review, partly to fix notation, the basic concepts and formulas regarding the emission of gravitational waves by binary systems, with emphasis on the effects produced by spins. We refer the reader to [33,34] for details and to [39] and references therein for a thorough review regarding post-Newtonian gravitational waveforms.

The whole *coalescence* of a binary system is usually divided into three distinct phases [40]: (i) the adiabatic inspiral, during which the BH orbital evolution occurs on the time scale of the gravitational radiation reaction, which is much longer than the orbital period; (ii) the merger, which takes place at the end of the inspiral when the binary orbit becomes relativistically unstable and the black holes enter a free fall plunge; and (iii) the ringdown, when the resulting BH settles down in its final stationary Kerr state, oscillating according to its normal modes. In this paper we consider only the inspiral phase. In fact the time to coalescence for a system radiating at frequency f is

$$\tau \simeq 1.2 \times 10^7 \left(\frac{f}{10^{-4} \text{ Hz}}\right)^{-8/3} \left(\frac{M(1+z)}{10^6 M_\odot}\right)^{-5/3} \left(\frac{\eta}{0.25}\right)^{-1} \text{ sec},$$

(14)

where M and η are the total mass and the symmetric mass ratio, respectively, defined in Eqs. (16b)–(16d), and τ is the *observed* lifetime of a binary system as recorded in the solar system for a source at redshift z with intrinsic total mass M that enters the detector window at the observed frequency $f = 10^{-4}$ Hz. Binary systems are therefore long lived in the LISA band, and one critically relies on long integration times to disentangle the sources parameters, in particular to resolve the source position in the sky and measure its luminosity distance [26].

As we consider only the inspiral phase of the coalescence, in the frequency domain we shut off the signal at frequency

$$f_{\text{isco}} = \frac{1}{\pi 6^{3/2} M(1+z)}$$

$$\simeq 4.4 \times 10^{-3} \left(\frac{M(1+z)}{10^6 M_\odot}\right)^{-1} \text{ Hz},$$

(15)

which corresponds to the innermost stable circular orbit of a particle orbiting a Schwarzichild black hole (ISCO). The real transition from inspiral to merger will occur at a frequency somewhat (by a factor $\lesssim 2$) different from f_{isco}, but due to the difficulty of defining the ISCO we will adopt the value (15). The results presented in this paper are anyway essentially unaffected by changing the cutoff frequency by a small factor.

We also assume the orbit to be circular. This is completely reasonable from an astrophysical point of view, as a massive binary system of roughly equal mass black holes has enough time—regardless of the initial eccentricity at which it

forms—to circularize before it enters the observational window, due to dynamical friction and radiation reaction [12,41].

A. Amplitude and phase evolution

We consider two massive black holes of mass m_1 and m_2 and spins $\mathbf{S}_1$ and $\mathbf{S}_2$, respectively. Several mass parameters are actually useful:

$$M = m_1 + m_2,$$

(16a)

$$\mu = \frac{m_1 m_2}{M},$$

(16b)

$$\mathcal{M} = \mu^{3/5} M^{2/5} = M \eta^{3/5},$$

(16c)

$$\eta = = \frac{\mu}{M};$$

(16d)

they represent, respectively, the total mass, the reduced mass, the chirp mass, and the symmetric mass ratio.

The system evolves by losing energy and angular momentum through emission of gravitational waves of increasing frequency and amplitude. The emitted radiation is given by the superposition of harmonics at multiples of the orbital period, and the two independent polarization amplitudes h_+ and $h_\times$ [42] can be schematically represented as [43]

$$h_{+,\times}(t) = \Re\left\{\sum_k H_{+,\times}^{(k)}(t) e^{ik\phi_{\text{orb}}(t)}\right\},$$

(17)

where $H_{+,\times}^{(k)}$ are time-dependent functions of the source parameters and $\phi_{\text{orb}}(t)$ is the binary orbital phase. The strongest harmonic is associated with the quadrupole moment of the source and therefore corresponds to $k = 2$. In this paper we consider the so-called *restricted post-Newtonian approximation* to the radiation (17): we retain only the leading order contribution to the amplitude, therefore only $H_{+,\times}^{(2)}$ at the Newtonian order, and take into account post-Newtonian corrections only to the phase of the signal $\phi(t) = 2\phi_{\text{orb}}(t)$. In this approximation Eq. (17) reads

$$h_+ = 2\frac{\mathcal{M}^{5/3}}{D_L}[1 + (\hat{\mathbf{L}} \cdot \hat{\mathbf{N}})^2](\pi f)^{2/3}\cos \phi(t),$$

(18a)

$$h_\times = -4\frac{\mathcal{M}^{5/3}}{D_L}(\hat{\mathbf{L}} \cdot \hat{\mathbf{N}})(\pi f)^{2/3}\sin \phi(t),$$

(18b)

where D_L is the source luminosity distance [44], $\hat{\mathbf{N}}$ the unit vector pointing toward the binary center of mass (in our convention the GW propagation direction is $-\hat{\mathbf{N}}$), and $\hat{\mathbf{L}}$ the orbital angular momentum unit vector.

We review now the expression for the GW phase $\phi(t)$. The signal frequency f, twice the orbital one, evolves according to [45]

$$\frac{df}{dt} = \frac{96}{5} \pi^{8/3} \mathcal{M}^{5/3} f^{11/3} \left[1 - \left(\frac{743}{336} + \frac{11}{4} \eta \right) (\pi M f)^{2/3} \right.$$

$$+ (4\pi - \beta)(\pi M f) + \left(\frac{34103}{18144} + \frac{13661}{2016} \eta \right.$$

$$+ \left. \frac{59}{18} \eta^2 + \sigma \right) (\pi M f)^{4/3} \Bigg], \tag{19}$$

where Eq. (19) is valid through the post²-Newtonian order and

$$\beta = \frac{1}{12} \sum_{i=1}^{2} \left[113 \left(\frac{m_i}{M} \right)^2 + 75 \eta \right] \left(\hat{\mathbf{L}} \cdot \frac{\mathbf{S}_i}{m_i^2} \right), \tag{20}$$

$$\sigma = \frac{\eta}{48} \left\{ -247 \left(\frac{\mathbf{S}_1}{m_1^2} \cdot \frac{\mathbf{S}_2}{m_2^2} \right) \right.$$

$$+ 721 \left. \left[\hat{\mathbf{L}} \cdot \frac{\mathbf{S}_1}{m_1^2} \right] \left[\hat{\mathbf{L}} \cdot \frac{\mathbf{S}_1}{m_1^2} \right] \right\} \tag{21}$$

are the so called *spin-orbit* and *spin-spin parameters*, respectively [45]. From Eq. (19) and $d\phi/dt = 2\pi f$, one can derive the time and phase evolution of the gravitational radiation:

$$t(f) = t_c - 5(8\pi f)^{-8/3} \mathcal{M}^{-5/3} \left[1 + \frac{4}{3} \left(\frac{743}{336} + \frac{11}{4} \eta \right) (\pi M f)^{2/3} \right.$$

$$- \frac{8}{5} (4\pi - \beta)(\pi M f) + 2 \left(\frac{3058673}{1016064} + \frac{5429}{1008} \eta + \frac{617}{144} \eta^2 \right.$$

$$- \left. \sigma \right) (\pi M f)^{4/3} \Bigg], \tag{22}$$

$$\phi(f) = \phi_c - \frac{1}{16} (\pi f \mathcal{M})^{-5/3} \left[1 + \frac{5}{3} \left(\frac{743}{336} + \frac{11}{4} \eta \right) (\pi M f)^{2/3} \right.$$

$$- \frac{5}{2} (4\pi - \beta)(\pi M f) + 5 \left(\frac{3058673}{1016064} \right.$$

$$+ \left. \frac{5429}{1008} \eta + \frac{617}{144} \eta^2 - \sigma \right) (\pi M f)^{4/3} \Bigg]; \tag{23}$$

t_c and ϕ_c, the *time* and *phase at coalescence*, are constants of integration, defined as the value of t and ϕ at (formally) $f = \infty$. As we mentioned, massive black holes spend months to years in the LISA observational window, depending on the mass. For future reference, if we assume that LISA observes the final year of inspiral of a binary, then the signal sweeps the frequency band between

$$f_a \simeq 4.2 \times 10^{-5} \left(\frac{T_{obs}}{1 \text{ yr}} \right)^{-3/8} \left[\frac{\mathcal{M}(1+z)}{10^6 M_\odot} \right]^{-5/8}, \tag{24}$$

which we call "arrival" (or "initial") frequency, and f_{isco}. An interesting quantity to consider is the total number of gravitational wave cycles recorded by the detector:

$$\mathcal{N}(t) = \frac{1}{2\pi} \int_{t_a}^{t} \phi(t') dt'. \tag{25}$$

From Eqs. (23) and (24), it is easy to compute the number of cycles in the final year of inspiral:

$$\mathcal{N} \approx 4.8 \times 10^2 \left(\frac{f_a}{10^{-4} \text{ Hz}} \right)^{-5/3} \left[\frac{\mathcal{M}(1+z)}{10^6 M_\odot} \right]^{-5/3}$$

$$\approx 2.1 \times 10^3 \left(\frac{T_{obs}}{1 \text{ yr}} \right)^{5/8} \left[\frac{\mathcal{M}(1+z)}{10^6 M_\odot} \right]^{-5/8}. \tag{26}$$

Table I contains reference values for f_a, f_{isco}, and $\mathcal{N}$ for a number of choices of masses and observation times.

B. Spin-induced precession

Present observations and theoretical prejudices suggest that massive black holes could be rapidly rotating. As we have mentioned in the previous section, if black holes are spinning, then the GW phase (23) contains two additional terms, one at the 1.5PN order, which is proportional to β, and the other at the 2PN order, which is proportional to σ. However, spins introduce a much more dramatic effect in the structure of the waveform, which is qualitatively different from the ones just mentioned: the orbital angular momentum $\mathbf{L}$ and the spins $\mathbf{S}_1$ and $\mathbf{S}_2$ change orientation due to the spin-orbit interaction (1.5PN effect), so that the radiation detected has a time varying polarization. $\mathbf{L}$, $\mathbf{S}_1$, and $\mathbf{S}_2$ process, over a time scale longer than the orbital period ($2/f \sim 30$ min) but shorter than the observation time (~ 1 yr), around the (almost) fixed direction of the total angular momentum $\mathbf{L} + \mathbf{S}_1 + \mathbf{S}_2$. This effect is actually quite dramatic and drastically changes the signature of the detected signal, as the orientation of the orbital plane changes during the year long observation time and the angular momenta complete several precession cycles around the fixed detection.

The spin-orbit-induced precession is the key new physical effect which is introduced in this paper. Here we review the main concepts and expressions and refer the reader to [33,34] for more details. In this paper we restrict our attention to the so-called *simple precession* [33], which takes place when (i) the BH masses are equal ($m_1 \sim m_2$) *or* (ii) one of the BHs has negligible spin (for convention, in this paper we shall assume $S_2 = 0$). Furthermore, one needs to impose the condition that the angular momenta be oriented so that $\mathbf{L} \neq -(\mathbf{S}_1 + \mathbf{S}_2)$. Under this assumptions the equations that describe the evolution of the angular momenta simplify considerably, and one can construct explicit analytical solutions for the relevant quantities. Moreover, the regime that we consider is well justified from an astrophysical point of view.

For circular orbits through the post¹·⁵-Newtonian order the equations describing the evolution of $\mathbf{L}$, $\mathbf{S}_1$, and $\mathbf{S}_2$ read

$$\dot{\hat{\mathbf{L}}} = \left[\frac{1}{r^3} \left(2 + \frac{3m_2}{2m_1} \right) \mathbf{J} \right] \times \hat{\mathbf{L}}, \tag{27}$$

TABLE I. Summary of the frequency band swept by massive black hole binary systems and the number of wave cycles recorded at the detector output in LISA observations for selected masses and integration times. The table shows the initial and final frequencies of the GWs, f_a and f_{isco}, respectively, the corresponding time of observation T_{obs}, and the number of waves cycles recorded at the output of the detector, coming from the various contributions of the terms in Eq. (23): Newtonian: the first term; post[1]-Newtonian (1PN): the second term, proportional to $(\pi M f)^{2/3}$; tail: $-10\pi(\pi M f)$; spin-orbit: $(5/2)\beta(\pi M f)$; post[2]-Newtonian (2PN): the last term, proportional to $(\pi M f)^{4/3}$ with $\sigma=0$; spin-spin: the $-5\sigma(\pi M f)^{4/3}$ term. The sources are selected with masses in the range $10^7 M_\odot - 10^5 M_\odot$; for each mass choice, three different f_a's are considered: the first corresponds to $T_{obs}=1$ yr, which does depend on m_1 and m_2, whereas the other two are the same for all m_1 and m_2, and correspond to $f_a=5\times10^{-5}$ Hz and 10^{-4} Hz, respectively. Notice that depending on f_a, m_1, and m_2, systems are observable for different times. The fiducial source is at $z=1$.

m_1 ($M_\odot$)	m_2 ($M_\odot$)	f_a ($\times10^{-4}$ Hz)	f_{isco} ($\times10^{-4}$ Hz)	T_{obs} (yr)	Newt.	1PN	tail	spin-orbit ($\times\beta$)	2PN	spin-spin ($\times\sigma$)
10^7	10^7	0.070	1.099	1.000	342	42	-40	3	3	-1
10^7	10^7	0.500	1.099	0.004	10	3	-5	0	1	0
10^7	10^6	0.153	1.999	1.000	761	87	-103	8	7	-2
10^7	10^6	0.500	1.999	0.038	96	22	-34	3	3	-1
10^7	10^6	1.000	1.999	0.005	23	7	-13	1	1	0
10^7	10^5	0.350	2.177	1.000	1792	290	-455	36	32	-10
10^7	10^5	0.500	2.177	0.366	949	187	-319	25	24	-8
10^7	10^5	1.000	2.177	0.045	238	65	-130	10	11	-4
10^7	10^4	0.776	2.196	1.000	4102	990	-1881	150	153	-51
10^7	10^4	0.500	2.196	3.649	9477	1834	-3160	252	235	-78
10^7	10^4	1.000	2.196	0.447	2383	647	-1296	103	110	-37
10^6	10^6	0.295	10.993	1.000	1453	102	-76	6	5	-1
10^6	10^6	0.500	10.993	0.246	602	59	-51	4	4	-1
10^6	10^6	1.000	10.993	0.038	187	28	-30	2	3	-1
10^6	10^5	0.647	19.987	1.000	3216	215	-201	16	11	-3
10^6	10^5	0.500	19.987	1.991	4950	280	-243	19	12	-4
10^6	10^5	1.000	19.987	0.312	1552	137	-144	11	9	-3
10^6	10^4	1.508	21.768	1.000	7571	748	-943	75	55	-18
10^6	10^4	0.500	21.768	19.285	48121	2366	-2176	173	96	-31
10^6	10^4	1.000	21.768	3.019	15096	1155	-1300	103	68	-22
10^5	10^5	1.242	109.929	1.000	6161	247	-141	11	8	-2
10^5	10^5	0.500	109.929	11.261	28097	618	-266	21	11	-2
10^5	10^5	1.000	109.929	1.781	8848	308	165	13	9	-2
10^5	10^4	2.729	199.872	1.000	13594	519	-374	30	16	-5
10^5	10^4	0.500	199.872	91.802	230221	2867	-1208	96	33	-9
10^5	10^4	1.000	199.872	14.494	72508	1430	-753	60	25	-7

$$\dot{\hat{\mathbf{S}}}=\left[\frac{1}{a^3}\left(2+\frac{3m_2}{2m_1}\right)\mathbf{J}\right]\times\hat{\mathbf{S}}, \qquad (28)$$

$$\frac{d}{dt}(\mathbf{S}_1\cdot\mathbf{S}_2)=0, \qquad (29)$$

$$\dot{S}=0, \qquad (30)$$

where

$$\mathbf{J}=\mathbf{L}+\mathbf{S}\quad(\mathbf{S}=\mathbf{S}_1+\mathbf{S}_2) \qquad (31)$$

is the conserved total angular momentum [46,47] (indeed $\dot{\mathbf{L}}=-\dot{\mathbf{S}}$).

Following [33], we highlight the main features of simple precession and provide, in a ready-to-use form, the relevant quantities needed for the computation of the LISA detector output. We will neglect the post[2]-Newtonian corrections, while retaining the post[1.5]-Newtonian terms (spin-orbit), which are dominant, for the $m_1=m_2$ case; they vanish anyway for $S_2=0$ [33,34].

One can summarize the main features of the *simple precession* as follows. $\hat{\mathbf{J}}$, $\hat{\mathbf{L}}$, and $\hat{\mathbf{S}}$ precess with the same angular velocity

$$\Omega_p=\left(2+\frac{3m_2}{2m_1}\right)\frac{J}{r^3} \qquad (32)$$

around the fixed direction

$$\hat{\mathbf{J}}_0=\hat{\mathbf{J}}-\epsilon\hat{\mathbf{J}}\times\hat{\mathbf{L}}, \qquad (33)$$

where

$$\epsilon \equiv \frac{L}{J}\frac{\dot{L}}{L\Omega_p} \ll 1. \tag{34}$$

The quantities $\mathbf{S}_1 \cdot \mathbf{S}_2$, $S = |\mathbf{S}_1 + \mathbf{S}_2|$, and

$$\kappa \equiv \hat{\mathbf{S}} \cdot \hat{\mathbf{L}} \tag{35}$$

are constant during the inspiral. The phase of the gravitational signal contains an additional contribution, the so-called "Thomas precession phase," given by [33]

$$\delta_p \phi(t) = -\int_t^{t_c} \delta_p \dot{\phi}(t') dt', \tag{36}$$

where

$$\delta_p \dot{\phi}(t) = \frac{\hat{\mathbf{L}} \cdot \hat{\mathbf{N}}}{1 - (\hat{\mathbf{L}} \cdot \hat{\mathbf{N}})^2}(\hat{\mathbf{L}} \times \hat{\mathbf{N}}) \cdot \dot{\hat{\mathbf{L}}}. \tag{37}$$

In analogy with the number of wave cycles, we can introduce here the number of precession cycles, $\mathcal{N}_p$, that $\hat{\mathbf{L}}$ and $\hat{\mathbf{S}}$ undergo around $\hat{\mathbf{J}}$ from some initial frequency f_a, at time t_a, to the final coalescence at t_c:

$$\mathcal{N}_p = \frac{1}{2\pi}\int_{t_a}^{t_c} \Omega_p(t) dt. \tag{38}$$

Depending on the mass ratio of a binary system, whether $m_1 \sim m_2$ ($L \gg S$) or $m_1 \gg m_2$ ($L \ll S$), $\mathcal{N}_p$ is well approximated by the expression

$$\mathcal{N}_p \approx \begin{cases} 10\left(1 + \dfrac{3m_2}{4m_1}\right)\left(\dfrac{m}{10^6 M_\odot}\right)^{-1}\left(\dfrac{f_a}{10^{-4}\ \mathrm{Hz}}\right)^{-1} & (L \gg S), \\[4mm] 2\left(1 + \dfrac{3m_2}{4m_1}\right)\left(\dfrac{m_1}{m_2}\right)\left(\dfrac{S}{m_1^2}\right)\left(\dfrac{m}{10^6 M_\odot}\right)^{-2/3}\left(\dfrac{f_a}{10^{-4}\ \mathrm{Hz}}\right)^{-2/3} & (L \ll S). \end{cases} \tag{39}$$

Notice that the precession cycles accumulate at low frequency, and for $L \gg S$, $\mathcal{N}_p$ does not depend on S; if $L \ll S$, $\mathcal{N}_p \propto (m_1/m_2) \gg 1$, which could therefore generate a very large number of precessions. In Table II we show the number of precession cycles, $\mathcal{N}_p$, and the value of the precession frequency Ω_p at f_a and f_{isco} for a number of choices of the mass of a binary system.

Using Eq. (32) we define now the *precession angle* α as

$$\frac{d\alpha}{dt} = \Omega_p. \tag{40}$$

From Eqs. (31), (33), and (35) it is straightforward to derive the relevant equations for the evolution of the total and orbital angular momentum:

$$\hat{\mathbf{J}} = \frac{\hat{\mathbf{L}} + \Upsilon \hat{\mathbf{S}}}{(1 + 2\kappa\Upsilon + \Upsilon^2)^{1/2}}, \tag{41a}$$

$$J = L(1 + 2\Upsilon + \Upsilon^2)^{1/2}, \tag{41b}$$

$$\dot{\hat{\mathbf{J}}} = \Upsilon\frac{\hat{\mathbf{S}}(1 + \Sigma\Upsilon) - \hat{\mathbf{L}}(\kappa - \Upsilon)}{(1 + 2\kappa\Upsilon + \Upsilon^2)^{3/2}}, \tag{41c}$$

$$\dot{\hat{\mathbf{L}}} = \Omega_p[\hat{\mathbf{J}}_0 \times \hat{\mathbf{L}} + \epsilon(\hat{\mathbf{J}}_0 \times \hat{\mathbf{L}}) \times \hat{\mathbf{L}}], \tag{41d}$$

$$\hat{\mathbf{L}} = \hat{\mathbf{J}}_0 \cos\lambda_L + \frac{\hat{\mathbf{z}} - \hat{\mathbf{J}}_0 \cos\theta_J}{\sin\theta_J}\sin\lambda_L \cos\alpha$$

$$+ (\hat{\mathbf{J}}_0 \times \hat{\mathbf{z}})\frac{\sin\lambda_L \sin\alpha}{\sin\theta_J}. \tag{41e}$$

In the previous equation θ_J and ϕ_J are the polar coordinates of $\hat{\mathbf{J}}_0$ in the fixed frame and

$$\lambda_L \equiv \arcsin\frac{|\dot{\hat{\mathbf{L}}}|}{\Omega_p} \tag{42}$$

is the angle between $\hat{\mathbf{L}}$ and $\hat{\mathbf{J}}$ (at the first order in ϵ, the approximation in which we are working, λ_L coincides with the angle between $\hat{\mathbf{L}}$ and $\hat{\mathbf{J}}_0$) and

$$\Upsilon(t) \equiv \frac{S}{L(t)}. \tag{43}$$

From Eqs. (32) and (34) one can write, explicitly,

$$\Omega_p = \left(2 + \frac{3m_2}{2m_1}\right)\frac{L}{r^3}\mathcal{G}, \tag{44}$$

$$\epsilon = \frac{16}{5}\left(\frac{m}{r}\right)^{3/2}\left[\left(1 + \frac{3m_2}{4m_1}\right)\mathcal{G}^2\right]^{-1}, \tag{45}$$

where

$$\mathcal{G}^2(f) \equiv 1 + 2\kappa\Upsilon + \Upsilon^2. \tag{46}$$

TABLE II. The total number of precession cycles, $\mathcal{N}_p$, and the precession angular frequency Ω_p at the beginning and end of LISA observations, for the final year of inspiral of a binary system at redshift $z=1$ with $\kappa=\hat{\mathbf{S}}\cdot\hat{\mathbf{L}}=0.9$ for selected values of the masses and spin magnitude.

m_1 ($M_\odot$)	m_2 ($M_\odot$)	S/M^2	Ω_p at f_a ($\times 10^{-4}$ Hz)	Ω_p at $f_{\rm isco}$ ($\times 10^{-4}$ Hz)	Number of precession cycles
10^7	10^7	0.95	0.009	1.254	11
10^7	10^7	0.50	0.007	0.892	9
10^7	10^7	0.10	0.005	0.579	7
10^7	10^6	0.95	0.008	1.043	11
10^7	10^6	0.50	0.005	0.632	7
10^7	10^6	0.10	0.003	0.272	4
10^7	10^5	0.95	0.026	0.911	34
10^7	10^5	0.50	0.014	0.489	19
10^7	10^5	0.10	0.003	0.114	5
10^7	10^4	0.95	0.133	0.895	127
10^7	10^4	0.50	0.064	0.472	71
10^7	10^4	0.10	0.012	0.096	15
10^6	10^6	0.95	0.018	12.540	25
10^6	10^6	0.50	0.015	8.919	20
10^6	10^6	0.10	0.013	5.788	16
10^6	10^5	0.95	0.015	10.432	23
10^6	10^5	0.50	0.011	6.319	16
10^6	10^5	0.10	0.007	2.716	9
10^6	10^4	0.95	0.047	9.110	74
10^6	10^4	0.50	0.025	4.892	40
10^6	10^4	0.10	0.007	1.144	11
10^5	10^5	0.95	0.038	125.396	54
10^5	10^5	0.50	0.034	89.194	46
10^5	10^5	0.10	0.030	57.877	39
10^5	10^4	0.95	0.030	104.315	48
10^5	10^4	0.50	0.023	63.186	34
10^5	10^4	0.10	0.016	27.159	22

Equations (43), (44), (45), and (46) can be used to integrate Eq. (40):

$$\alpha = \alpha_c - \frac{96}{5\mu^3 m^3}\left(1+\frac{3m_2}{4m_1}\right)\left[2(\mathcal{G}L)^3 - 3\kappa S(L+\kappa S)\mathcal{G}L\right.$$
$$\left. - 3\kappa S^3(1-\kappa^2)\text{arcsinh}\left(\frac{L+\kappa S}{S(1-\kappa^2)^{1/2}}\right)\right]. \quad (47)$$

In Eq. (47) the angle α_c is a constant of integration that essentially identifies the position of $\hat{\mathbf{L}}$ and $\hat{\mathbf{S}}$ on the precession cone at the reference time t_c. Finally, the frequency evolution of λ_L—the angle between $\hat{\mathbf{L}}$ and $\hat{\mathbf{J}}$ changes with time—is given by

$$\sin\lambda_L = \frac{\Upsilon(1-\kappa^2)^{1/2}}{(1+2\kappa\Upsilon+\Upsilon^2)^{1/2}} = \frac{S(1-\kappa^2)^{1/2}}{L(f)\mathcal{G}(f)}, \quad (48a)$$

$$\cos\lambda_L = \frac{1+\kappa\Upsilon}{(1+2\kappa\Upsilon+\Upsilon^2)^{1/2}} = \frac{L(f)+\kappa S}{L(f)\mathcal{G}(f)}. \quad (48b)$$

Notice that at 1.5PN order, which corresponds to the post-Newtonian order at which we model the waveform in this paper, the contribution of the spins to the GW phase (23) depends only on the parameter β. However, if one takes into account the change of orientation of the angular momenta, then the spin-orbit coupling is described by three parameters—say, α_c, κ, and S—on which β depends. In the implementation of the computation of the Fisher information matrix (cf. Sec. V), we found it convenient to use as independent parameters β, κ, and α_c.

IV. OBSERVED SIGNAL

We can now derive ready-to-use analytical expressions for the signal measured by LISA at the Michelson detector output, Eq. (7), when the source is an inspiraling binary system of spinning massive black holes. In this case, as a result of the relativistic spin-orbit coupling, the binary angular momenta $\mathbf{L}$, $\mathbf{S}_1$, and $\mathbf{S}_2$ precess, following the equations described in Sec. III B. It is worth spelling out the assumption under which the signal is derived: (i) the binary is in circular orbit; (ii) the waveform is modeled using the restricted post$^{1.5}$-Newtonian approximation (amplitude at the lowest quadrupole Newtonian contribution, and GW phase at the 1.5PN order); (iii) the masses and/or spins are such that the system undergoes "simple precession."

In the most general case the signal depends on 17 parameters: two mass parameters, six parameters related to the BH spins—the magnitude and orientation of each spin—the orbital eccentricity, the luminosity distance (which is a *direct observable* in GW astronomy), two angles identifying the location of the source in the sky, two angles that describe the orientation of the orbital plane, one angle that describes the orientation of the ellipse in the orbital plane, an arbitrary reference time—say, the time at coalescence—and the signal phase at that time. In the approximation that we consider here the signal depends on 12 unknown parameters (cf. the next section for more details). The key new qualitative feature that we introduce here and that is not present in any of the previous analysis [26,27,29,30] is the change of orientation of the orbital angular momentum during the observation. Unlike the model considered in [27,29], here we consider only the waves emitted at twice the orbital frequency.

Before providing the explicit expression for $h(t)$, it is worth summarizing the key motions and the associated time scales that affect the detector output.

(i) LISA orbits around the Sun, so that the barycenter of the instrument changes position over the time scale of one sidereal year: this motion Doppler-shifts the incoming gravitational waves and depends only on the source position in the sky;

(ii) The orientation of the LISA arms changes over the same time scale because the detector precesses around the normal to the ecliptic: this introduces a phase and amplitude modulation which is due to the time-dependent response of

the detector to the two orthogonal polarizations h_+ and $h_\times$; this effect depends on both the position and orientation of the source in the sky.

(iii) The binary orbital plane changes orientation in the sky with **L** and **S** that precess around the total angular momentum **J**, whose direction is essentially constant. The time scale of precession is longer than the orbital period but much shorter than the LISA rotation time scale and depends on both the source-detector relative orientation and the binary physical parameters (masses and spins): the incoming GWs are therefore *intrinsically* modulated in amplitude and phase.

We consider first the representation of detector output in the time domain $h^{(\iota)}(t)$; we will then turn to the frequency domain representation $\tilde{h}^{(\iota)}(f)$.

A. Measured signal in the time domain

In the amplitude-and-phase representation, the signal $h^{(\iota)}(t)$ [cf. Eq. (7)] measured by the ιth Michelson LISA interferometer and produced by the polarization amplitudes (18a) and (18b) reads

$$h^{(\iota)}(t) = A(t)A_p^{(\iota)}(t)\cos[\phi(t) + \delta_p\phi(t) + \varphi_p^{(\iota)}(t) + \varphi_D(t)]. \tag{49}$$

In the previous expression,

$$A_p^{(\iota)}(t) = \frac{\sqrt{3}}{2}\{[1 + (\hat{\mathbf{L}}\cdot\hat{\mathbf{N}})^2]^2 F_+^{(\iota)}(t)^2 + 4(\hat{\mathbf{L}}\cdot\hat{\mathbf{N}})^2 F_\times^{(\iota)}(t)^2\}^{1/2}, \tag{50}$$

$$\varphi_p^{(\iota)}(t) = \tan^{-1}\left\{\frac{2(\hat{\mathbf{L}}\cdot\hat{\mathbf{N}})F_\times^{(\iota)}(t)}{[1 + (\hat{\mathbf{L}}\cdot\hat{\mathbf{N}})^2]F_+^{(\iota)}(t)}\right\} \tag{51}$$

are the *polarization amplitude* and *phase*, respectively;

$$\varphi_D(t) = 2\pi R_\oplus f \sin\theta_N \cos[\Phi(t) - \phi_N] \quad (R_\oplus = 1 \text{ AU}) \tag{52}$$

is the *Doppler phase modulation* induced by the motion of the LISA detector around the Sun; $\delta_p\phi(t)$ is the so-called *Thomas precession phase*, Eq. (36), which vanishes for spinless binary systems; the amplitude of the gravitational wave signal is

$$A[t(f)] = 2\frac{\mathcal{M}^{5/3}}{D}[\pi f(t)]^{2/3}, \tag{53}$$

and the GW phase $\phi(t)$ is given by Eq. (23), where at 1.5PN order one neglects the term proportional to $(\pi M f)^{4/3}$.

The structure of $h^{(\iota)}(t)$ clearly shows that the signal measured at the detector output is phase and amplitude modulated because of the three effects that we have mentioned above:

(i) the orbital motion of the instrument around the Sun which Doppler modulates, through φ_D, the phase of the incoming gravitational wave signal; this effect is the same for $h^{(I)}$ and $h^{(II)}$; (ii) the change of orientation of the detector during the time of observation that through $F_+^{(\iota)}(t)$ and $F_\times^{(\iota)}(t)$ affects $A_p^{(\iota)}$ and $\varphi_p^{(\iota)}$, in different ways depending on

ι; (iii) the change of $\hat{\mathbf{L}}$ due to the spin-orbit interaction which affects $A_p^{(\iota)}$ and $\varphi_p^{(\iota)}$ through $(\hat{\mathbf{N}}\cdot\hat{\mathbf{L}})$ and ψ_N' [cf. Eqs. (8a), (8b), (12), (50), and (51)]; the impinging signal is *intrinsically* modulated. Furthermore, $\delta_p\phi$ adds to the phase of the signal.

In order to complete the analysis of the detector output, we need to provide explicit expressions for $(\hat{\mathbf{L}}\cdot\hat{\mathbf{N}})$, which enters Eq. (50) and (51), and $(\hat{\mathbf{L}}\cdot\hat{\mathbf{z}}')$ and $[\hat{\mathbf{N}}\cdot(\hat{\mathbf{L}}\times\hat{\mathbf{z}}')]$, which are needed to compute ψ_N', Eq. (12), and therefore the antenna beam patters. Using Eqs. (4) and (41e) we obtain

$$\hat{\mathbf{L}}\cdot\hat{\mathbf{N}} = (\hat{\mathbf{J}}_0\cdot\hat{\mathbf{N}})\cos\lambda_L + \frac{\cos\theta_N - (\hat{\mathbf{J}}_0\cdot\hat{\mathbf{N}})\cos\theta_J}{\sin\theta_J}$$
$$\times\sin\lambda_L\cos\alpha + \frac{(\hat{\mathbf{J}}_0\times\hat{\mathbf{z}})\cdot\hat{\mathbf{N}}}{\sin\theta_J}\sin\lambda_L\sin\alpha, \tag{54}$$

$$\hat{\mathbf{L}}\cdot\hat{\mathbf{z}}' = (\hat{\mathbf{J}}_0\cdot\hat{\mathbf{z}}')\cos\lambda_L$$
$$+ \frac{1 - 2(\hat{\mathbf{J}}_0\cdot\hat{\mathbf{z}}')\cos\theta_J}{2\sin\theta_J}\sin\lambda_L\cos\alpha$$
$$+ \frac{(\hat{\mathbf{J}}_0\times\hat{\mathbf{z}})\cdot\hat{\mathbf{z}}'}{\sin\theta_J}\sin\lambda_L\sin\alpha, \tag{55}$$

$$\hat{\mathbf{N}}\cdot(\hat{\mathbf{L}}\times\hat{\mathbf{z}}') = \hat{\mathbf{N}}\cdot(\hat{\mathbf{J}}_0\times\hat{\mathbf{z}}')\cos\lambda_L$$
$$+ \frac{\hat{\mathbf{N}}\cdot(\hat{\mathbf{z}}\times\hat{\mathbf{z}}') - \hat{\mathbf{N}}\cdot(\hat{\mathbf{J}}_0\times\hat{\mathbf{z}}')\cos\theta_J}{\sin\theta_J}\sin\lambda_L\cos\alpha$$
$$+ \frac{\hat{\mathbf{N}}\cdot(\hat{\mathbf{J}}_0\times\hat{\mathbf{z}})\times\hat{\mathbf{z}}'}{\sin\theta_J}\sin\lambda_L\sin\alpha. \tag{56}$$

In the previous expressions $\sin\lambda_L$, $\cos\lambda_L$ and α are given by Eqs. (48a), (48b), and (47), respectively, and the remaining quantities describing the orientation of the source with respect of the detector read

$$\hat{\mathbf{J}}_0\cdot\hat{\mathbf{z}}' = \frac{1}{2}\cos\theta_J - \frac{\sqrt{3}}{2}\sin\theta_J\cos[\Phi(t) - \phi_J], \tag{57}$$

$$\hat{\mathbf{J}}_0\cdot\hat{\mathbf{N}} = \cos\theta_J\cos\theta_N + \sin\theta_J\sin\theta_N\cos(\phi_J - \phi_N), \tag{58}$$

$$\hat{\mathbf{N}}\cdot(\hat{\mathbf{J}}_0\times\hat{\mathbf{z}}') = \frac{1}{2}\sin\theta_N\sin\theta_J\sin(\phi_J - \phi_N) - \frac{\sqrt{3}}{2}\cos\Phi(t)$$
$$\times(\cos\theta_J\sin\theta_N\sin\phi_N - \cos\theta_N\sin\theta_J\sin\phi_J)$$
$$- \frac{\sqrt{3}}{2}\sin\Phi(t)(\cos\theta_N\sin\theta_J\cos\phi_J$$
$$- \cos\theta_J\sin\theta_N\cos\phi_N), \tag{59}$$

$$\hat{\mathbf{N}}\cdot(\hat{\mathbf{J}}_0\times\hat{\mathbf{z}}) = \sin\theta_N\sin\theta_J\sin(\phi_J - \phi_N), \tag{60}$$
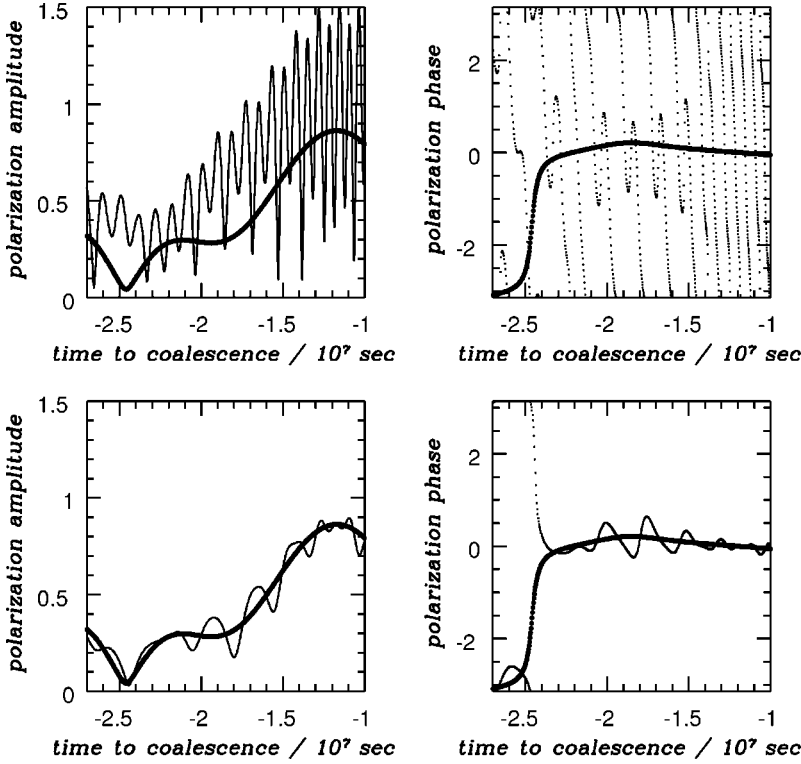
FIG. 1. The evolution of the polarization amplitude (left panels) and phase (right panels), computed according to Eqs. (50) and (51), for the final year of inspiral of a binary system as a function of time. The bold solid line refers to black holes with no spin, the dotted line (for the phase) and thin solid-line (for the amplitude) to spinning objects. The relevant source parameters are chosen as follows: $m_1 = 10^7 M_\odot$, $m_2 = 10^5 M_\odot$, $S/m^2 = 0.95$, and $\hat{\mathbf{S}} \cdot \hat{\mathbf{L}} = 0.5$ (top panels) and $m_1 = m_2 = 10^6 M_\odot$, $S/m^2 = 0.3$, and $\hat{\mathbf{S}} \cdot \hat{\mathbf{L}} = 0.9$ (bottom panels). The location and initial orientation of the source have been chosen randomly. See the text for further details.

$$\hat{\mathbf{N}} \cdot (\hat{\mathbf{z}} \times \hat{\mathbf{z}}') = \frac{\sqrt{3}}{2} \sin \theta_N \sin[\Phi(t) - \phi_N], \qquad (61)$$

$$\hat{\mathbf{J}} \cdot (\hat{\mathbf{z}} \times \hat{\mathbf{z}}') = \frac{\sqrt{3}}{2} \sin \theta_J \sin[\Phi(t) - \phi_J], \qquad (62)$$

$$\hat{\mathbf{N}} \cdot (\hat{\mathbf{J}}_0 \times \hat{\mathbf{z}}) \times \hat{\mathbf{z}}' = -\frac{1}{2} \sin \theta_J \{ \sqrt{3} \cos \theta_N \cos[\Phi(t) - \phi_J]$$

$$+ \sin \theta_N \cos(\phi_J - \phi_N) \}. \qquad (63)$$

Last, we need to compute the scalar and vector products necessary to derive the Thomas precession phase $\delta_p \phi(t)$, Eqs. (36) and (37):

$$(\hat{\mathbf{L}} \times \hat{\mathbf{N}}) \cdot \dot{\hat{\mathbf{L}}} = \Omega_p [\cos \lambda_L (\hat{\mathbf{N}} \cdot \hat{\mathbf{L}}) - (\hat{\mathbf{N}} \cdot \hat{\mathbf{J}}_0) - \epsilon \hat{\mathbf{J}}_0 \cdot (\hat{\mathbf{L}} \times \hat{\mathbf{N}})],$$
$$(64)$$

$$\hat{\mathbf{J}}_0 \cdot (\hat{\mathbf{L}} \times \hat{\mathbf{N}}) = \frac{\hat{\mathbf{N}} \cdot (\hat{\mathbf{J}}_0 \times \hat{\mathbf{z}})}{\sin \theta_J} \sin \lambda_L \cos \alpha$$

$$+ \frac{\cos \theta_J (\hat{\mathbf{N}} \cdot \hat{\mathbf{J}}_0) - \cos \theta_N}{\sin \theta_J} \sin \lambda_L \sin \alpha; \qquad (65)$$

$\delta_p \phi(t)$ can be therefore computed using Eqs. (47), (48a), (48b), (54), (57), (58), and (59).

An example of the LISA output when black holes rapidly spin is shown in Fig. 1, where we plot the amplitude and phase modulation, Eqs. (50) and (51), during the final year of inspiral. Two cases are actually presented: a binary system

with $m_1 = 10^7 M_\odot$, $m_2 = 10^5 M_\odot$, $S/m^2 = 0.95$, and $\hat{\mathbf{S}} \cdot \hat{\mathbf{L}} = 0.5$ and an equal mass binary where the parameters correspond to $m_1 = m_2 = 10^6 M_\odot$, $S/m^2 = 0.3$, and $\hat{\mathbf{S}} \cdot \hat{\mathbf{L}} = 0.9$. The evolution of $A_p(t)$ and $\varphi_p(t)$ for the two sets of physical parameters is compared to the spinless case. A simple eye inspection shows how dramatic is the effect induced by spins, and it should therefore not come as a surprise that the errors associated with the measurements of the source parameters are strongly affected.

B. Measured signal in the frequency domain

For several applications in data analysis, it is often more useful to work in the frequency domain, and we will derive now an approximation to the Fourier representation of the signal $h^{(\iota)}(t)$, Eq. (49). Our convention for the Fourier transform $\tilde{g}(f)$ of any real function $g(t)$ is

$$\tilde{g}(f) = \int_{-\infty}^{\infty} e^{2\pi i f t} g(t) dt. \qquad (66)$$

The Fourier transform (66) of the signal $h^{(\iota)}(t)$ can be computed in an rather straightforward way using the stationary phase approximation (see [52]) and considering the gravitational waveform $A(t) \cos \phi(t)$ in Eq. (49) as the *carrier signal* modulated by the motion of the detector and the source's orbital plane [26,33]. Under this assumption, the Fourier transform of the detector output (49) reads

$$\tilde{h}^{(\iota)}(f) \simeq \begin{cases} \mathcal{A}A_p^{(\iota)}[t(f)]f^{-7/6}e^{\{i[\Psi(f)-\varphi_p^{(\iota)}[t(f)]-\varphi_D[t(f)]-\delta_p\phi[t(f)]]\}}, & 0<f\leqslant f_{\text{isco}}, \\ 0, & f>f_{\text{isco}}, \end{cases} \tag{67}$$

where

$$\mathcal{A} = \left(\frac{5}{96}\right)^{1/2}\pi^{-2/3}\frac{\mathcal{M}^{5/6}}{D}, \tag{68}$$

$$\Psi(f)=2\pi f t_c - \phi_c - \frac{\pi}{4} + \frac{3}{4}(8\pi\mathcal{M}f)^{-5/3}$$

$$\times\left[1+\frac{20}{9}\left(\frac{743}{336}+\frac{11}{4}\eta\right)(\pi mf)^{2/3}\right.$$

$$-4(4\pi-\beta)(\pi mf)+10\left(\frac{3058673}{1016064}+\frac{5429}{1008}\eta\right.$$

$$\left.+\frac{617}{144}\eta^2 - \sigma\right)(\pi mf)^{4/3}\right]. \tag{69}$$

Notice that in Eq. (69) the term proportional to $(\pi mf)^{4/3}$ corresponds to the post^2-Newtonian order and will not be considered in this work.

V. PARAMETER ESTIMATION

In this section we discuss the errors associated to the parameter measurement when LISA monitors binary systems of rapidly rotating massive black holes in circular orbit. We start by briefly recalling the general concepts and formulas regarding parameter estimation—we refer the reader to [48–52] and references therein for more details—and then present the results of our analysis applied to LISA data.

A. Review of signal analysis and parameter estimation

The signal $s(t)$ registered at the detector output is the superposition of noise $n(t)$ and gravitational waves $h(t;\boldsymbol{\lambda})$:

$$s(t)=h(t;\boldsymbol{\lambda})+n(t); \tag{70}$$

$\boldsymbol{\lambda}$ represents the vector of the unknown parameters (location, masses, spins, etc.) that characterize the actual waveform and that one wishes to estimate from the data stream. We assume the noise to be stationary and Gaussian, characterized by a noise spectral density $S_n(f)$. In the geometrical approach to signal processing it is useful to consider $s(t)$ as a vector in the signal vector space and to introduce the following inner product between two signals v and w [52]:

$$(v|w)=2\int_0^\infty \frac{\tilde{v}(f)\tilde{w}^*(f)+\tilde{v}^*(f)\tilde{w}(f)}{S_n(f)}df. \tag{71}$$

According to the definition (71), the optimal signal-to-noise ratio (SNR) at which h can be detected is

$$S/N=\frac{(h|h)}{\text{rms}[(h|n)]}=(h|h)^{1/2}. \tag{72}$$

In this paper we discuss the errors associated with the measurement of the unknown parameter vector $\boldsymbol{\lambda}$ that characterizes the signal $h(t;\boldsymbol{\lambda})$. In the limit of large SNR, which is clearly the case for LISA observations of massive black hole binary systems, the errors $\Delta\boldsymbol{\lambda}$ follow a Gaussian probability distribution:

$$p(\Delta\boldsymbol{\lambda})=\left(\frac{\det(\boldsymbol{\Gamma})}{2\pi}\right)^{1/2}e^{-\Gamma_{jk}\Delta\lambda^j\Delta\lambda^k/2}. \tag{73}$$

In Eq. (73) the matrix Γ_{jk} is known as the Fisher information matrix and reads

$$\Gamma_{jk}^{(\iota)}\equiv\left(\frac{\partial h^{(\iota)}}{\partial\lambda^j}\bigg|\frac{\partial h^{(\iota)}}{\partial\lambda^k}\right). \tag{74}$$

The *variance-covariance matrix* is simply given by the inverse of the Fisher information matrix:

$$\Sigma^{jk}=\langle\Delta\lambda^j\Delta\lambda^k\rangle=[(\boldsymbol{\Gamma}^{(\iota)})^{-1}]^{jk}. \tag{75}$$

The matrix $\boldsymbol{\Sigma}$ contains full information about the parameter errors and their correlations and is what we need to compute (cf. next section) in order to investigate the LISA parameter estimation. In fact the diagonal elements of $\boldsymbol{\Sigma}$ represent the expected mean-square errors

$$\langle(\Delta\lambda^j)^2\rangle=\Sigma^{jj}, \tag{76}$$

and its off-diagonal elements provide information about the correlations among different parameters through the correlation coefficients c^{jk}:

$$c^{jk}=\frac{\Sigma^{jk}}{\sqrt{\Sigma^{jj}\Sigma^{kk}}} \quad (-1\leqslant c^{jk}\leqslant+1). \tag{77}$$

In the limit of high signal-to-noise ratio, Σ^{jj} provides a tight lower bound to the minimum mean-square error $\langle(\Delta\lambda^j)^2\rangle$, the so-called Cramer-Rao bound [49,50]. It is important to notice that the errors (76) and the correlation coefficients (77) depend both on the actual value of the signal parameter vector $\boldsymbol{\lambda}$. For the case of observations with two or more detectors with uncorrelated noise, the Fisher information matrix is simply $\Gamma_{jk}=\Sigma_\iota\Gamma_{jk}^{(\iota)}$.

One of the properties that we are interested in is the angular resolution of the instrument, which we define as

$$\Delta\Omega_N=2\pi\{\langle\Delta\cos\theta_N^2\rangle\langle\Delta\phi_N^2\rangle-\langle\Delta\cos\theta_N\Delta\phi_N\rangle^2\}^{1/2}. \tag{78}$$

The physical meaning of $\Delta\Omega_N$ is the following: the probability of the source to lie *outside* an (appropriately shaped) error ellipse enclosing a solid angle $\Delta\Omega$ is simply $e^{-\Delta\Omega/\Delta\Omega_N}$.

B. LISA observations

We discuss now how accurately LISA can measure the source parameters in the case of rapidly spinning black holes. The goal of this section is to investigate whether spins, which have been neglected in studies carried out so far, can significantly affect the estimation of the source parameters. A thorough exploration of this effect requires to probe a very large multidimensional parameter space, and it is well outside of the scope of this paper. Here we concentrate on a fiducial source of two $10^6 M_\odot$ black holes at redshift $z=1$— a rather typical LISA source—and we compare the errors associated with the parameter measurements in the case in which spins are present—for large spins $S/M^2=0.95$ and moderate spins $S/M^2=0.3$; in both cases $\kappa=0.9$—and the case where spins are neglected (the black holes are considered, *a priori*, to be not spinning).

Before presenting the results we spell out the assumptions under which we compute the errors (76).

(i) The orbit is circular; we regard such a hypothesis as realistic, as we are dealing with massive systems of black holes of comparable mass. As the orbit shrinks due to dynamical friction the eccentricity is likely to decrease [11–13] and the radiation reaction completes the circularization process before GWs enter the observational window of LISA; in fact the eccentricity e evolves according to $e \propto f^{-19/18}$ [41].

(ii) The black holes are spinning, so that the binary orbit precesses in space. However, in order to simplify the description of the precession motion, still addressing a realistic astrophysical scenario, we assume that either $m_1=m_2$ (the case considered in this paper) or $S_2=0$ and the spins and angular momentum are not antialigned. Under this conditions a binary undergoes the so-called simple precession [33], and the equations describing the evolution of the relevant physical quantities simplify considerably (cf. Sec. III B for more details).

(iii) We restrict the analysis only to the inspiral phase of the whole coalescence. We approximate the waveform $\tilde{h}^{(\iota)}(f;\lambda)$ at the restricted 1.5PN order. The GW signal detected at the LISA output is therefore described by Eqs. (67), (68), and (69). Because we retain terms up to 1.5PN order in the GW phase, in the expression of $\Psi(f)$, Eq. (69), we neglect the last term proportional to $(\pi M f)^{4/3}$. We shut off the inspiral waveform at the frequency $f_{\rm isco}$, given by Eq. (15). In the computation of the errors (76) we actually neglect the Thomas precession phase $\delta_p(t)$, Eq. (36). This simplification is motived by computational reasons and does not affect in any significant way the final results. In fact, $\delta_p[t(f)]$ must be computed numerically at each frequency using the past history of the binary; $\delta_p[t(f)]$ needs then to be included in the integrand of the scalar product (71) that leads to determination of the elements of the Fisher information matrix. This double numerical integration, which needs to be carried out to high accuracy in order to keep under control numerical instabilities that occur otherwise in the numerical inversion

of Γ_{jk}, makes the computational time very long, due to our limited computational resources. We have checked for a few (random) choices of the source parameters that including $\delta_p[t(f)]$ does not change in any appreciable way the result. This is to be expected. For the physical parameters considered in this paper the Thomas precession phase contribute to ≈ 1 wave cycle, out of a total ≈ 1500. It also represents a secular increase in the phase of the GW signal, qualitatively not different from the one given by $\Psi(f)$.

(iv) We consider the fiducial sources to be at redshift $z=1$ [55]. As the systems are at cosmological distance, the values of all the physical parameters entering the GW signal presented in the previous sections must be considered as the *observed ones*; they differ from the values of the parameters as measured in the source rest frame by a factor $(1+z)$; the parameters are "Doppler shifted" according to:

$$f \rightarrow \frac{f}{(1+z)},$$

$$t \rightarrow (1+z)t,$$

$$\mathcal{M} \rightarrow (1+z)\mathcal{M},$$

$$m \rightarrow (1+z)m,$$

$$\mu \rightarrow (1+z)\mu. \qquad (79)$$

(v) We assume that the instrument observes the whole final year of inspiral; the GWs sweep therefore the frequency band between the *arrival frequency* $f_{\rm a}$ and the final cutoff frequency $f_{\rm isco}$; $f_{\rm a}$ is determined so that after 1 yr, as measured by an observer in our solar system, the GW instantaneous frequency reaches $f_{\rm isco}$:

$$T_{\rm obs} = t(f_{\rm isco}) - t(f_{\rm a})$$

$$= 1 \ \ {\rm yr} = 3.1556926 \times 10^7 \ \ {\rm sec.} \qquad (80)$$

The range $f_{\rm a} \leq f \leq f_{\rm isco}$ determines the integration domain in Eq. (74); values of $f_{\rm a}$ and $f_{\rm isco}$ for selected choices of the source parameters are given in Table I. Note that we do not impose a low-frequency cutoff to LISA; this choice is based on the fact that the real low-frequency noise wall of space-based instruments is not very well understood at the moment, placed somewhere in the range 10^{-5}–10^{-4} Hz.

(vi) The total noise that affects the observations is given by the superposition of instrumental sources and astrophysical foregrounds of unresolved radiation due to (mainly) galactic white dwarf binary systems [53,54], the so-called "confusion noise." The total noise spectral density $S_n(f)$ is therefore the sum of these two components, and we use the analytical approximations given in [26,55] .

(vii) Out of the 17 parameters on which the most general waveform depends, the signal $\tilde{h}^{(\iota)}(f;\lambda)$ that we consider here depends on 12 independent parameters. In our analysis we adopt the following choice of independent parameters: $\ln\mathcal{M}$ and $\ln\mu$ (mass parameters), $\cos\theta_N$, ϕ_N, $\cos\theta_J$, ϕ_J,
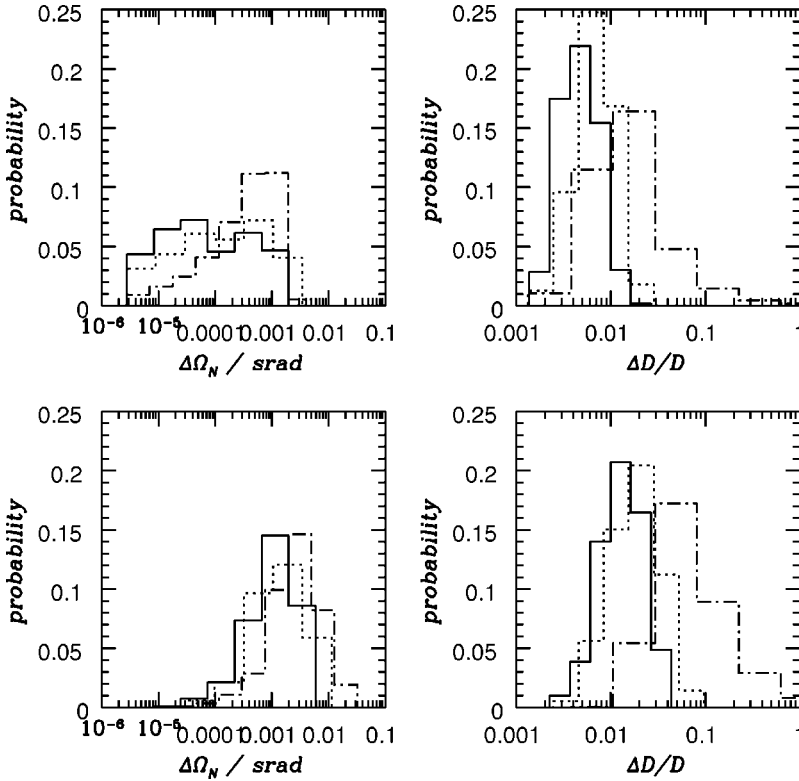
FIG. 2. The probability distribution of $\Delta\Omega_N$ (left) and $\Delta D_L/D_L$ (right), for observations of the final year of inspiral of a binary system with $m_1=m_2=10^6\ M_\odot$ at $z=1$. The histograms show the result of a Monte Carlo simulation, where 1000 sources have been randomly located and oriented in the sky. The bottom panels refer to measurements carried out with only one detector, whereas the top panels describe the results obtained by combining the two independent data streams. The plots compare the errors for different values of the BH spins: $S/m^2=0.9$ (solid line), 0.3 (dotted line), and 0 (dot-dashed line).

and α_c (geometry of the binary with respect to the detector), κ and β (spin parameters), $\ln D_L$ (distance of the source), and finally t_c and ϕ_c.

(viii) We compute the expected mean square errors $(\langle\Delta\lambda_j^2\rangle)^{1/2}$ and the angular resolution $\Delta\Omega_N$ for the case of observations carried out with one detector and with combined observations of both detectors I and II. The analysis is done in the frequency domain: we first compute analytically the derivatives $\partial h^{(\iota)}/\partial\lambda^j$, where $j=1,\ldots,12$, then compute numerically Γ_{jk} and Σ^{jk}, Eqs. (74) and (75); the integration and matrix inversion are performed using numerical routines of the NAG library.

LISA parameter estimation strongly depends (the results vary by orders of magnitude) on the actual value of the signal parameters. In particular, one of the key set of parameters that affect the errors is the location and orientation of a source with respect to the detector. This represents already a large parameter space that one needs to explore in order to obtain meaningful results. We perform this exploration by means of Monte Carlo simulations, which therefore affect the way in which the results are presented, given in terms of probability distributions. For each set of physical parameters, we select randomly the five geometrical parameters (θ_N, ϕ_N, θ_J, ϕ_J, and α_c) from a uniform distribution in $\cos\theta_N$, ϕ_N, $\cos\theta_J$, ϕ_J, and α_c. The Monte Carlo simulation is done on 1000 different sets of angles. As far as the other seven parameters are concerned we chose them as follows. We consider a fiducial source at redshift $z=1$, with $m_1=m_2=10^6 M_\odot$ (which sets the three parameters D_L, $\mathcal{M}$, and μ), with $t_c=\phi_c=0$. We fix the *tilt angle* parameter $\kappa=0.9$, and we explore three different values of the size of the spin S: (i) $S/M^2=0.95$, (ii) $S/M^2=0.3$, and (iii) $S=0$. No-

tice that given m_1, m_2, S, and κ we can easily derive β. It is worth noticing that in this paper we do not explore the effect of the tilt angle $\cos^{-1}\kappa$, which is also likely to affect the errors. Such analysis is currently in progress [37]. We would also like to stress that for the case $S=0$ the waveform that we actually consider is the one corresponding to the nonprecessing restricted 2PN approximation (this is the waveform used in [30], very similar to the one used in [26], which is the nonprecessing restricted 1.5PN approximation). This is equivalent to assuming that we know *a priori* that spins are zero and the binary system does no precess. Note that this is different from estimating the source parameters using the waveform (67) where precession is included, and assuming $S\ll1$. In the case $S=0$ we need to estimate only 11 parameters, and not 12. The reason of this choice is to compare existing results in the literature with our new ones that take into account spin-orbit modulations.

Figures 2, 3, and 4 summarize the key results. Figures 2 and 3 show the probability distribution of the parameter errors, for $\Delta\Omega_N$, $\Delta D_L/D_L$, $\Delta\mathcal{M}/\mathcal{M}$, and $\Delta\mu/\mu$. Figure 4 shows the cumulative probability distributions: if we define $\xi\equiv\Delta\lambda^j$, the plots show $P(\xi<\xi_0)=\int_0^{\xi_0}p(\xi')d\xi'$ as a function of ξ_0. Each plot compares the nonspinning case with the cases in which the black holes are spinning with two different value of the spins, $S/M^2=0.95$ and 0.3.

The key result, which is absolutely clear from Figs. 2, 3, and 4 is that the errors in the spinning case are smaller than in the nonspinning one, even if the number of parameters that one needs to estimate is greater (12 instead of 11). One can intuitively understand this behavior by looking at Fig. 1, which shows the amplitude and phase evolution of the signal
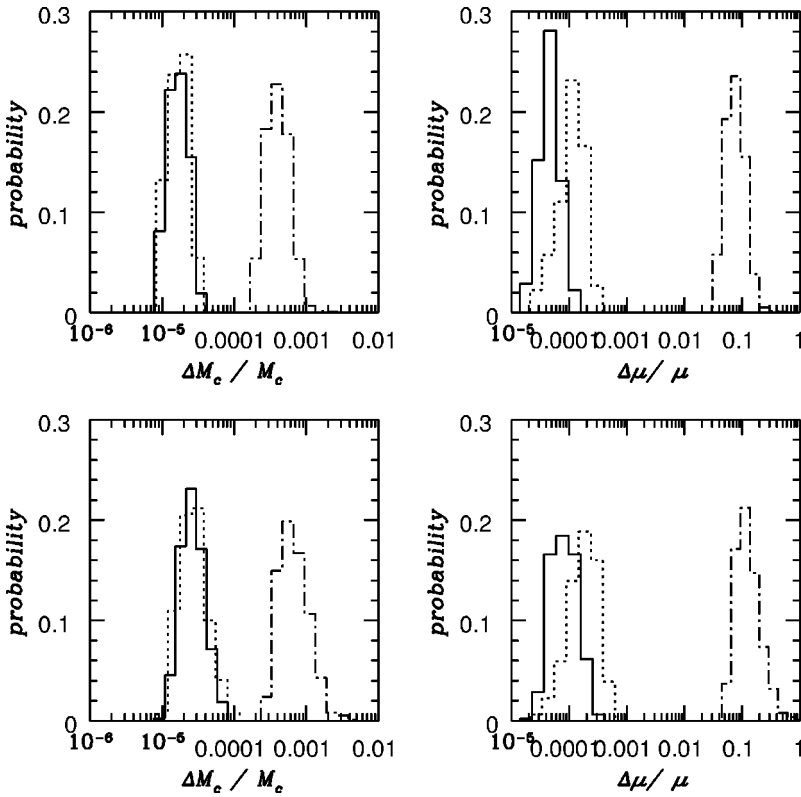
FIG. 3. The probability distribution of $\Delta \mathcal{M}/\mathcal{M}$ (left) and $\Delta \mu/\mu$ (right) for observations carried out with only one interferometer (bottom) and the two combined LISA outputs (top). The parameters are the same as in Fig 2.

recorded at the LISA output: precessing binaries show a much greater richness of features than nonspinning sources. These are the features that help in measuring the parameters.

However, despite all the parameters being estimated with smaller errors with respect to the nonspinning case, there is

striking difference between the ''position parameters''— location in the sky and luminosity distance—and mass parameters. In fact, the errors $\Delta \Omega_N$ and $\Delta D_L/D_L$ are reduced by a factor of 2–10 depending on the actual value of the source parameter. We know that LISA reconstructs the posi-
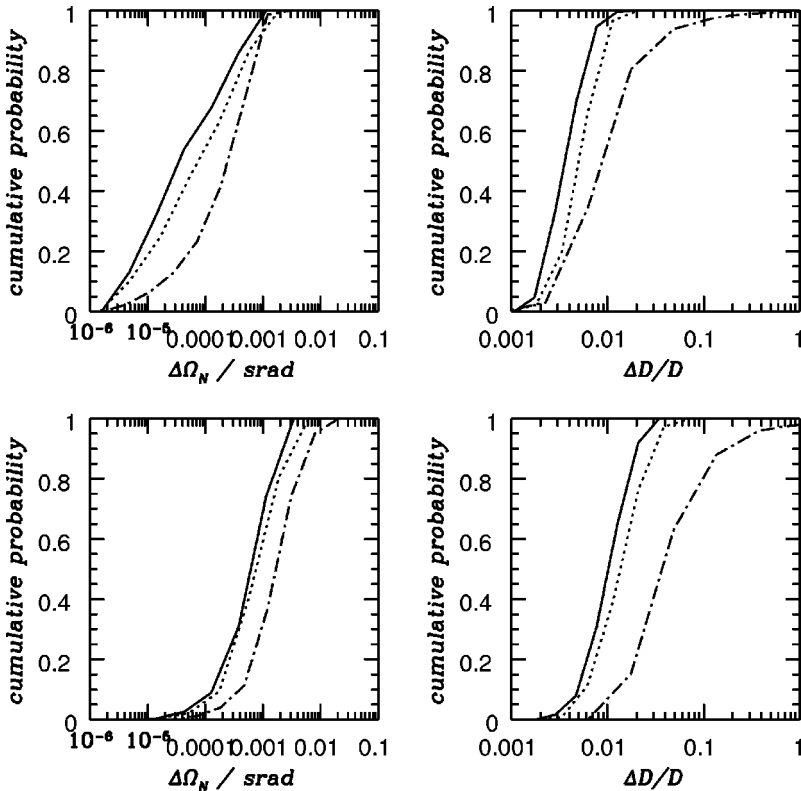

FIG. 4. Same as Fig. 2, but now the cumulative probability distributions as a function of the parameters $\Delta \Omega_N$ and $\Delta D_L/D_L$ are shown. See text for more details.

tion of the source in the sky by exploiting the modulation in the amplitude and phase of the signal, and precession introduces one additional modulation effect which can improve the determination of $\hat{\mathbf{N}}$ and decorrelates D_L from $\mathcal{M}$, which improves the measurement of the luminosity distance. Still, the change of position and orientation of LISA is the main effect that allows the source to be located. The improvement in $\Delta\Omega_N$ and $\Delta D_L/D_L$ is, however, significant: the fraction of sources that can be located within, say, one square degree is 10% for nonspinning binaries, 35% for binaries with 0.3, and 50% with 0.95 (for $\kappa=0.9$). The systems whose distance is known to better than 1% is about 60% for nonspinning binaries and essentially the totality for spinning binaries.

The situation is radically different for the masses: in the nonspinning case the instrument reconstructs the value of the two mass parameters by staying in phase with the GW phase, whose time evolution is mainly controlled by $\mathcal{M}$ (the leading Newtonian term) and, to a less extent, by μ, through the post-Newtonian corrections [cf. Eqs. (23) and (69) and Table I]. $\mathcal{M}$ and μ play no role in the amplitude and phase modulation, $A_p(t)$ and $\varphi_p(t)$, Eqs. (50) and (51). As a consequence, $\mathcal{M}$ is measured much more accurately, by a factor of ~ 100 or more, than μ (see Fig. 3 and [26,30]). If spins are present, the masses start to play a role also in $A_p(t)$ and $\varphi_p(t)$, because they control the rate at which $\mathbf{L}$ and $\mathbf{S}$ precess, and therefore are responsible for the intrinsic amplitude and phase modulation of the signal. This has two effects on the parameter estimation: it decorrelates $\mathcal{M}$ from μ (at the Newtonian order the two mass parameters are even degenerate) and provides new features in the measured signal that improve the parameter estimation. The net effect is that the errors in $\mathcal{M}$ and μ are now of the same order, with a drastic improvement with respect to the nonspinning case, of by a factor of ~ 50 and $\sim 10^3$ for $\Delta\mathcal{M}/\mathcal{M}$ and $\Delta\mu/\mu$, respectively; $\Delta\mathcal{M}/\mathcal{M}$ is still ≈ 3 times smaller than $\Delta\mu/\mu$, due to the role played by $\mathcal{M}$ in the GW phase $\phi(t)$. It also clear that the additional signature produced by the masses on the amplitude and phase modulation helps in removing the correlation between $\mathcal{M}$ and D_L, therefore reducing $\Delta D_L/D_L$, as we have already mentioned.

To summarize, the parameters of two 10^6 $M_\odot$ black holes spiraling toward the final merger at $z=1$ and rapidly rotating—say, $S/M^2=0.95$ and $\kappa=0.9$—can be measured very accurately: $\mathcal{M}$ and μ can be measured to a few parts in 10^5, the luminosity distance to better than 1% (in some cases almost 0.1%), and with an error box in the sky 10^{-6} srad $\lesssim \Delta\Omega_N \sim 10^{-3}$ srad. Notice that the errors scale with the distance roughly as $\Delta\Omega_N \sim 1/D_L^2$ and $\Delta\mathcal{M}/\mathcal{M} \sim \Delta\mu/\mu \sim \Delta D_L/D_L \sim 1/D_L$. This would be strictly true for white noise, which is not the case for LISA. In particular going to higher redshift, one can expect a degradation of the measurements more severe than the one predicted by this simple scaling, because GWs are redshifted to lower frequencies where the noise is higher and some initial portion of the signal falls out of the observational window.

For multiband, electromagnetic, and gravitational observations of the same event the key parameter is the instrument's angular resolution. In fact there is some hope that

LISA will have enough angular resolution to locate the galaxy or galaxy cluster where a coalescence of massive black holes takes place; this would enable other telescopes to be pointed at the same area of the sky and to observe the aftermath of such catastrophic event. However, previous studies [26,27,29,30] have concluded that this might actually be impossible for sources at $z \approx 1$ (or beyond), because of the poor angular resolution of GW observations. In short, the results of our analysis suggest that in some exceptional case LISA might be able to identify the host galaxy cluster of a MBH binary of 10^6 $M_\odot$ at $z=1$, but in general the LISA error box will contain several hundreds of galaxy clusters and $\gtrsim 10^5$ galaxies, all of them potential hosts of a LISA detected source. Such a conclusion can be easily derived by comparing the LISA angular resolution with the one of other telescopes and the angular size of galaxies at high redshift. An optical telescope, such as the Keck telescope, has a field of view of about 1 square degree. Chandra has a square field of view of 16×16 arcmin with a spatial resolution of $\simeq 1$ arcsec, and XMM has a circular field of view with radius 15 arcmin and a spatial resolution of a few arcsec. INTEGRAL has an even wider circular field of view—the radius is 10 deg—with a poorer spatial resolution (12 arcmin). There is therefore no doubt that, for a typical LISA source at $z=1$, GW observations will provide information accurate enough to cover the interesting portion of the sky with a single observation by one of (or all) the former instruments. At $z=1$, the typical size of a galaxy is $\simeq 3$ arcsec and the typical size of a galaxy cluster is $\simeq 2$ arcmin. In a very few lucky occasions LISA will be able to detect a source with $\Delta\Omega_N \approx 3\times 10^{-3}$ deg^2, but more typically the angular resolution is $\Delta\Omega_N \approx 0.3$ deg^2, and could be much worse for a few detections ($\Delta\Omega_N \approx 5$ deg^2). It is therefore clear that for the "high-spatial-resolution" GW detections, only ≈ 3 galaxy clusters will fall in the LISA error box, but more typically the number of clusters will be ≈ 300. If there is still a small (but not negligible) chance of identifying the galaxy cluster hosting a GW source, the chances of pinpointing the host galaxy seem to be very bleak (the former numbers need to be multiplied by a factor $\sim 10^3$ for galaxies).

VI. CONCLUSION

We have considered LISA observations of massive black hole binary systems in the final stage of inspiral for rapidly rotating black holes. We have restricted our analysis to comparable mass objects in circular orbit, modeling the radiation at the restricted post$^{1.5}$-Newtonian order assuming simple precession. We have derived ready-to-use analytical expressions for the signal registered at the detector output, both in the time and frequency domains, and have determined the mean-square errors associated with the parameter measurements for equal mass 10^6 $M_\odot$ binary systems at $z=1$ for selected spin parameters and a wide range of source locations and orientations. Our analysis clearly shows that the presence of spins reduces (by orders of magnitude, for some parameters) the errors with which the source parameters are measured. LISA is therefore a more powerful telescope than previously thought if spins play a significant role. The main

shortcoming of our analysis is the limited region of the parameter space that we have been able to explore, which is entirely due to our limited computational resources. Such analysis is currently in progress [37]. Of particular interest is the exploration of the parameter space in the case where the masses are not comparable—i.e., where the mass ratio is ~ 0.1 or smaller. Our present understanding of the relevant astrophysical scenarios suggests, in fact, that the formation of unequal mass binaries should be regarded as the rule rather than the exception. When the mass ratio increases, the number of precession cycles detected at the LISA output will increase as well [cf. Table II and Eq. (39)]. It is therefore conceivable that precession will be even more effective in breaking the degeneracy among the parameters, in particular the two masses. However, the amount of intrinsic rotation S shall also play a crucial role, as the number of precession cycles is proportional to S. Preliminary results suggest that

for $m_2/m_1 = 0.1$ and rapidly rotating systems ($S/M^2 \approx 0.9$) the estimation of the mass parameters and the angular resolution improve by a factor of a few, with respect to the equal mass case, provided that the signal-to-noise ratio is not strongly affected. In general, in fact, unequal mass systems will be detected at a lower SNR, so that precession compensates for the loss of SNR. The latter eventually dominates the effect of rotation when m_2/m_1 decreases further and compromises the accuracy with which parameters can be measured.

[1] P. L. Bender *et al.*, "LISA Pre-Phase A Report," 2nd ed., MPQ 233, 1998; P. L. Bender *et al.*, "LISA – System and Technology Study Report," ESA-SCI(2000)11, 2000. http://www.lisa.jpl.gov

[2] C. Cutler and K.S. Thorne, "An Overview of Gravitational-Wave Sources," gr-qc/0204090.

[3] J. Magorrian *et al.*, Astrophys. J. **115**, 2285 (1998).

[4] D. Richstone *et al.*, Nature (London) **395**, A14 (1998).

[5] R. Genzel, A. Eckart, T. Ott, and F. Eisenhauer, Mon. Not. R. Astron. Soc. **291**, 219 (1997).

[6] M. Miyoshi, J. Moran, J. Herrnstein, L. Greenhill, N. Nakai, P. Diamond, and M. Inoue, Nature (London) **373**, 127 (1995).

[7] E. Maoz, Astrophys. J. Lett. **494**, L181 (1998).

[8] X. Fan *et al.*, Astrophys. J. **122**, 2833 (2001).

[9] J.S.B. Wyithe and A. Loeb, Astrophys. J. **581**, 886 (2002).

[10] D. Merritt and L. Ferrarese, Astrophys. J. **547**, 140 (2001).

[11] M.C. Begelman, R.D. Blandford, and M.J. Rees, Nature (London) **287**, 307 (1980).

[12] A. Vecchio, M. Colpi, and A. Polnarev, Astrophys. J. **433**, 733 (1994).

[13] M. Rajagopar and R.W. Romani, Astrophys. J. **446**, 543 (1995).

[14] M. Milosavljevic and D. Merritt, Astrophys. J. **563**, 34 (2001).

[15] Q. Yu, Mon. Not. R. Astron. Soc. **331**, 935 (2002).

[16] A. Gould and H. Rix, Astrophys. J. Lett. **532**, L29 (2000).

[17] P.J. Armitage and P. Natarajan, Astrophys. J. Lett. **567**, L9 (2002).

[18] M.G. Haehnelt, Mon. Not. R. Astron. Soc. **269**, 199 (1994).

[19] M.G. Haehnelt, in *Laser Interferometer Space Antenna*, edited by W. M. Falkner, AIP Conf. Proc. No. **456** (AIP, Woodbury, NY, 1998), pp. 45–49.

[20] A. Vecchio, Class. Quantum Grav. **14**, 1431 (1997).

[21] K. Menou, Z. Haiman, and V.K. Narayanan, Astrophys. J. **558**, 535 (2001).

[22] K. Menou, Class. Quantum Grav. **20**, 537 (2003).

[23] A.H. Jaffe and D.C. Backer, Astrophys. J. **583**, 616 (2003).

[24] J.S.B. Wyithe and A. Loeb, Astrophys. J. **590**, 691 (2003).

[25] T. Pursimo *et al.*, Astron. Astrophys., Suppl. Ser. **146**, 141 (2000).

[26] C. Cutler, Phys. Rev. D **57**, 7089 (1998).

[27] A. M. Sintes and A. Vecchio, in *Gravitational Waves—Third Amaldi Conference*, edited by S. Meshkov (AIP, Melville, NY, 2000), pp. 403–404.

[28] A. M. Sintes *et al.* (in preparation).

[29] T.A. Moore and R.W. Hellings, Phys. Rev. D **65**, 062001 (2002).

[30] S. Hughes, Mon. Not. R. Astron. Soc. **331**, 805 (2002).

[31] N. Seto, Phys. Rev. D (to be published).

[32] S.A. Hughes and R.D. Blandford, Astrophys. J. Lett. **585**, L101 (2003).

[33] T.A. Apostolatos, C. Cutler, G.S. Sussman, and K.S. Thorne, Phys. Rev. D **49**, 6274 (1994).

[34] L.E. Kidder, Phys. Rev. D **52**, 821 (1995).

[35] A. Vecchio and C. Cutler, in *Laser Interferometer Space Antenna* [19], pp. 101–109.

[36] A. Vecchio, in *Gravitational Waves—Third Amaldi Conference* [27], pp. 238–247.

[37] A. Vecchio *et al.* (in preparation).

[38] We would like to caution the reader of the different notation used in this paper with respect to [26]: the reference frames (x,y,z) and (x',y',z') of this paper coincide, respectively, with the frames $(\bar{x},\bar{y},\bar{z})$ and (x,y,z) of [26].

[39] L. Blanchet, Living Review in Relativity 2002-3 http://www.livingreviews.org/Articles/Volume5/2002-3blanchet/index.html, 2002.

[40] E.E. Flanagan and S. Hughes, Phys. Rev. D **57**, 4535 (1998).

[41] P.C. Peters, Phys. Rev. **136**, B1224 (1964).

[42] K. S. Thorne, in *300 Years of Gravitation*, edited by S. W. Hawking and W. Israel (Cambridge University Press, Cambridge, England, 1987), pp. 330–458.

[43] L. Blanchet, B.R. Iyer, C.M. Will, and A.G. Wiseman, Class. Quantum Grav. **13**, 575 (1996).

[44] S. Weinberg, *Gravitation and Cosmology: Principles and Applications of the General Theory of Relativity* (Wiley, New York, 1972).

[45] L. Blanchet, T. Damour, B.R. Iyer, C.M. Will, and A.G. Wiseman, Phys. Rev. Lett. **74**, 3515 (1995).

[46] B.M. Barker and R.F. O'Connell, Phys. Rev. D **12**, 329 (1975).

[47] K.S. Thorne and J.B. Hartle, Phys. Rev. D **31**, 1815 (1985).

[48] L. A. Wainstein and V. D. Zubakov, *Extraction of Signals from Noise* (Dover, New York, 1962).

[49] C. W. Helstrom, *Statistical Theory of Signal Detection*, 2nd ed. (Pergamon Press, London, 1968).

[50] D. Nicholson and A. Vecchio, Phys. Rev. D **57**, 4588 (1998).

[51] L.S. Finn, Phys. Rev. D **46**, 5236 (1992).

[52] C. Cutler and E.E. Flanagan, Phys. Rev. D **49**, 2658 (1994).

[53] D. Hils, P.L. Bender, and R.F. Webbink, Astrophys. J. **360**, 75 (1990).

[54] P.L. Bender and D. Hils, Class. Quantum Grav. **14**, 1439 (1997).

[55] In this paper we are mainly concerned with a comparison of the errors obtained without considering spins with the ones that are given when spins are included in the signal. It is therefore clear that the actual redshift (distance) of the fiducial source and the choice of the expected noise spectral density (instrumental noise and confusion noise) have little interest, as far as the same values are used in the two cases.